Title:

Disrupted resting-state fMRI coherence links carotid artery stenosis to functional connectivity loss in humans

Short title:

Disrupted resting-state fMRI coherence in carotid artery stenosis

Authors:

Sangcheon Choi[1,2,8], Gabriel Hoffmann[1,2], Sebastian Schneider[1,2], Stephan Kaczmarz[1,2,3], Xin Yu[4], Christine Preibisch[1,2,5,7], and Christian Sorg[1,2,6,7]

Affiliations:

1 Institute for Neuroradiology, School of Medicine and Health, TUM University Hospital, Technical University of Munich, Munich 81675, Germany

2 TUM-Neuroimaging Center, School of Medicine and Health, Technical University of Munich, Munich 81675, Germany

3 Philips GmbH Market DACH, Hamburg 22335, Germany

4 Athinoula A. Martinos Center for Biomedical Imaging, Department of Radiology, Harvard Medical School, Massachusetts General Hospital, Charlestown, MA 02129, USA

5 Clinic for Neurology, School of Medicine and Health, TUM University Hospital, Technical University of Munich, Munich 81675, Germany

6 Clinic for Psychiatry, School of Medicine and Health, TUM University Hospital, Technical University of Munich, Munich 81675, Germany

7 These authors contributed equally to this work.

8 Lead Contact

***Lead corresponding author:**

Dr. Sangcheon Choi

Email: sc.choi@tum.de
Address: Ismaninger Str. 22, 81675 Munich, Germany
Phone: +49 0152 26330531

Keywords: vasomotion, cerebrovascular disease, functional connectivity, multimodal imaging

ABSTRACT

Vasomotor dynamics at infra-slow frequencies (~0.1 Hz), driven by synchronized oscillations of smooth muscle cells in vessel walls, play a crucial role in regulating cerebral perfusion and underlie resting-state functional connectivity (FC). Animal studies have shown that vasomotor activity contributes to coherent blood oxygenation level dependent (BOLD) signal fluctuations. However, in humans, detecting this contribution non-invasively remains challenging due to the limited spatiotemporal sensitivity of functional magnetic resonance imaging (fMRI) to vasomotion. Given that prior studies have identified ICAS as an informative conditional lesion model of vasomotor and hemodynamic impairments in humans, we investigated whether vasomotor dysfunction affects interhemispheric BOLD coherence at ~0.1 Hz. Using a multi-modal fMRI framework integrating resting-state fMRI with quantitative mapping of cerebral blood volume, blood flow, oxygen metabolism, and BOLD time lag, we compared BOLD coherence between patients with unilateral ICAS and healthy controls. Frequency-specific analysis revealed significantly diminished interhemispheric BOLD coherence at ~0.1 Hz across canonical resting-state networks in ICAS patients, while ultra-slow (<0.05 Hz) coherence remained largely preserved. This reduction was spatially widespread and particularly pronounced in watershed areas, i.e., border zones between major vascular territories, associated with significantly increased lateralization of cerebral blood volume ($p < 0.01$). Notably, coherence-based FC patterns at ~0.1 Hz were heterogeneous within watershed areas but homogeneous outside, suggesting an interplay between compensatory mechanisms and vasomotor impairment. Taken together, our findings demonstrate that frequency-resolved, region-specific analysis can capture 0.1 Hz-specific oscillatory signals and detect subtle alterations in interhemispheric FC, offering a non-invasive biomarker for early cerebrovascular dysfunction, particularly in ICAS.

INTRODUCTION

Vasomotor activity, arising from synchronized oscillations of smooth muscle cells in vascular walls, has been implicated in changes in arteriole diameter (1-6). These oscillatory vasomotor signals reflect underlying vascular conditions and have been widely observed across species, including humans (1, 2, 7-16). In animals, invasive techniques such as laser Doppler flowmeter and optical recording have demonstrated that cerebral vasomotor activity typically exhibits slow oscillations peaking around 0.1 Hz within the infra-slow fluctuations (4, 5, 9, 10, 12, 16). Importantly, beyond its established role in regulating local cerebral perfusion, vasomotor activity has also been proposed as a physiological basis for functional connectivity (FC) during resting-state (5). This hypothesis is primarily supported by evidence that spontaneous vasomotor oscillations, synchronized across homotopic cortical regions (i.e., symmetric regions in both hemispheres) and induced by ongoing neuronal activity, contribute to coherent blood oxygenation dependent level (BOLD) functional magnetic resonance imaging (fMRI) signals underlying resting-state FC in awake rodents as demonstrated by invasive optical imaging (5, 6, 16). Coherence-based analysis has further demonstrated that spontaneous arteriole diameter oscillations, driven by vasomotion (~0.1 Hz) in the infra-slow fluctuations, can modulate BOLD fMRI signal coherence, particularly in homotopic cortical regions (5, 6). Notably, a distinct peak in power spectral density (PSD) near 0.1 Hz has been observed in the somatosensory cortex of anesthetized rats, suggesting that inter-hemispheric FC can be strengthened through vasomotion-related mechanisms (17, 18).

However, in humans, the contributions of vasomotion to resting-state BOLD FC remain insufficiently elucidated, primarily due to technical challenges in measuring vasomotion non-invasively and the presence of Mayer waves in the same frequency band (~0.1 Hz) (19, 20). Under intraoperative conditions, a few invasive human studies have reported spatially distinct vasomotor oscillations across the cortex at the vasomotor frequency (~0.1 Hz) (7, 15). Despite these observations, evidence linking vasomotor activity to resting-state BOLD FC in humans using non-invasive fMRI remains scarce (11, 14, 15). Vasomotor activity, which regulates the arterial reservoir volume (1), is considered ubiquitous in vascular structures (16) and may serve as a potential biomarker of cerebrovascular dysfunction. Indeed, disrupted vasomotor activity has been observed in both high-risk stroke mouse models (21) and in patients with internal carotid artery stenosis (ICAS) (22-26). Given the evidence of vasomotor impairment in patients with ICAS, it is plausible that inter-hemispheric resting-state (rs-) fMRI coherence, particularly in the ~0.1 Hz frequency band, may be altered in patients with ICAS and could serve as a frequency-specific signature of cerebrovascular dysfunction. Nevertheless, no direct model of vasomotor dynamics for FC currently exists in humans. Although prior studies have suggested that ICAS can be considered a natural lesion model of vasomotor dysfunctions (22-26), its impact is not limited to vasomotion. ICAS is also associated with hemodynamic impairments (i.e., perfusion alterations) (27-32) that influence BOLD FC. Therefore, ICAS represents an informative conditional lesion model of impaired vasomotion in humans.

Moreover, multi-parametric hemodynamic MRI studies have revealed unilateral vascular-hemodynamic impairments in CBF and cerebral blood volume (CBV) in patients with asymptomatic unilateral ICAS (27-32), while the cerebral metabolic rate of oxygen ($CMRO_2$) remains largely preserved, suggesting intact neuronal function (33). The most pronounced alterations in CBF and CBV have been observed in watershed areas, i.e., cortical and internal border zones between major perfusion territories that are particularly vulnerable to hypoperfusion (28), suggesting that vasomotor activity may be reflected in macroscopic CBV

measures (34-36). In addition, disrupted coupling between CBF and $CMRO_2$ has been reported in the ICAS patients, indicating altered flow-metabolism dynamics (30). Although correlation-based rs-fMRI analyses have shown that vasomotor impairment is strongly associated with decreased FC in patients with high-grade ICAS (26), minimal or no group-level differences in homotopic correlation between healthy controls and ICAS patients (after controlling for hemodynamic impairments) suggest that vascular-hemodynamic impairments may influence resting-state FC in more subtle or complex ways (31, 32).

Taken together, these findings suggest that inter-hemispheric coherence of rs-fMRI signals in patients with asymptomatic unilateral ICAS may be altered in both frequency-specific and spatially dependent ways. We therefore hypothesize that vasomotor impairments in these patients lead to spectrally and spatially specific alterations in inter-hemispheric resting-state BOLD FC. Furthermore, we propose that frequency-resolved coherence analysis can uncover subtle but meaningful disruptions in brain networks that may not be detectable using conventional correlation methods, thereby providing new insights into the physiological basis of FC in the human brain. Our investigation is guided by three central hypotheses regarding the impact of unilateral ICAS: 1) Frequency specificity: We hypothesize that the most prominent alterations in BOLD signal oscillations and coherence will occur in the ~0.1 Hz frequency range (particularly 0.08-0.1 Hz (11, 15, 37), see **Discussion**), which has been associated with vasomotion (5, 26), whereas ultra-slow coherence below 0.05 Hz, reflecting neuronal activity (34) and arousal brain state (38) will remain largely preserved. 2) Brain-wide effect: We hypothesize that vasomotion-related disruptions in inter-hemispheric coherence will be spatially widespread across the whole brain (11, 14, 16). 3) Regional vulnerability: We hypothesize that disrupted BOLD signal fluctuations, inter-hemispheric coherence alterations, and corresponding changes in vasomotion-related hemodynamic parameters, particularly CBV, will be concentrated in vulnerable vascular territories such as watershed areas, which have been previously demonstrated to be most affected by hypoperfusion (28, 39, 40).

In this study, we combined rs-fMRI with quantitative hemodynamic MRI to investigate how asymptomatic unilateral ICAS alters frequency-specific inter-hemispheric BOLD signal coherence and its coupling to cerebral perfusion parameters. To test our hypotheses, we developed a novel analytic framework integrating rs-fMRI-based spectral power spectral density (PSD) and coherence analysis with multi-parametric MRI maps including relative CBV, CBF, relative $CMRO_2$, and BOLD time lag (i.e., relative time lag of cortical regions to the sagittal superior sinus) in both healthy controls and patients with unilateral ICAS, particularly inside watershed areas as well as across resting-state brain networks. To assess frequency specificity (hypothesis 1), we compared inter-hemispheric PSD and coherence between healthy controls and patients with asymptomatic unilateral ICAS across distinct frequency bands (<0.05 Hz and ~0.1 Hz) and across both homotopic and heterotopic regions of interest (ROI) pairs. To assess brain-wide effects (hypothesis 2), we analyzed inter-hemispheric coherence patterns across intrinsic resting state networks defined by Yeo and colleagues (41). Finally, to assess regional vulnerability (hypothesis 3), we compared inter-hemispheric PSD, coherence, and quantitative hemodynamic parameters between regions of distinct perfusion (8), specifically inside versus outside watershed areas, i.e., vascular border zones that are particularly vulnerable to reductions in CBF in patients with ICAS (28). Our findings not only offer new insights into the impact of vascular impairment on frequency-resolved brain network dynamics and distinct perfusion territories but also highlight the potential of inter-hemispheric coherence at vasomotor frequencies as a distinct, non-invasive biomarker for early cerebrovascular dysfunction.

RESULTS

Frequency-specific disruption of inter-hemispheric BOLD coherence at ~0.1 Hz in patients with unilateral ICAS

We developed a multi-modal fMRI approach to assess whole-brain BOLD rs-fMRI signals and multi-parametric quantitative hemodynamic MRI maps to test our hypotheses in healthy controls and patients with asymptomatic unilateral ICAS (**Fig. 1A**). For inter-hemispheric ROI-based analysis, we employed an Atlas of Intrinsic Connectivity of Homotopic Areas (AICHA) (42), extracting fMRI time series from individual AICHA-defined ROIs (**Fig. 1B-C**). To test our first hypothesis that inter-hemispheric rs-fMRI coherence may be impaired in the vasomotor frequency band (~0.1 Hz, i.e., 0.08-0.1 Hz) (5), we compared power spectral densities (PSDs) across hemispheres, as well as inter-hemispheric coherence, between healthy controls and patients with unilateral ICAS across the infra-slow oscillatory frequency band (<0.1 Hz). Using the AICHA atlas (42) (**Fig. 1B**), we first analyzed the temporal oscillatory patterns and frequency responses of rs-fMRI signals between the right (ipsilateral to the stenosis in patients) and left hemispheres. In representative subjects from each group, we computed the ROI-average, Z-score normalized rs-fMRI time series for both hemispheres and compared the correlation and coherence values between them. As illustrated in **Fig. 1D** and **G**, the patient with ICAS exhibited weaker synchronization and less pronounced oscillatory patterns, resulting in lower correlation and coherence values, compared to the healthy control. To investigate alterations in inter-hemispheric FC in patients with ICAS, we analyzed Z-score normalized rs-fMRI time series for homotopic and heterotopic AICHA ROI pairs in the representative subjects shown in **Fig. 1G**. Based on correlation coefficients from the representative healthy control, we selected two AICHA ROI pairs, i.e., #1: Precuneus, #2: Lingual (**Fig. 1E-F**), which showed the highest homotopic correlation. We first examined homotopic rs-fMRI time series from the Precuneus ROI pair and compared correlation and coherence values between the two signals. As shown in **Fig. 1H**, the ICAS patient (right) exhibited synchronized but visibly weaker oscillatory temporal patterns compared to the healthy control (left). While the correlation coefficients were identical (control: 0.95; patient: 0.95), the coherence was notably reduced in the patient (control: 0.93; patient: 0.88), suggesting frequency-specific decoupling between the two hemispheres. Next, we assessed heterotopic rs-fMRI time series from the Precuneus and Lingual ROIs. As illustrated in **Fig. 1I**, the ICAS patient (right) showed markedly reduced synchronized and oscillatory temporal patterns, with both correlation and coherence values lower than those observed in the healthy control (left; correlation: control 0.72 vs. patient 0.53, coherence: control 0.51 vs. patient 0.40). These findings suggest that ICAS may differentially influence inter-hemispheric FC relying on the spatial relationship and spectral dynamics of the ROI pair.

To examine group-level frequency-specific effects, we computed PSDs separately for the right and left hemispheres. Both groups exhibited robust PSD peaks at 0.01-0.05 Hz (referred to as <0.05 Hz; **Fig. 1J**). However, in the ICAS group, a distinct alteration of PSD in the 0.08-0.1 Hz range (referred to as ~0.1 Hz; **Fig. 1J**) was noted, potentially reflecting reduced vasomotor activity or other potential confounders (see **Discussion**). Intriguingly, peaks at ~0.02 Hz appeared only in ICAS patients, although this was not statistically significant (not shown), suggesting a potential spectral shift toward lower frequency (6, 43). To statistically assess hemispheric difference, we calculated the absolute inter-hemispheric differences in PSDs ($|\Sigma(\Delta_{LR}\ PSD)|$) for both frequency bands (<0.5 Hz and ~0.1 Hz). Notably, a significant group difference emerged in the slow oscillatory frequency band, ~0.1 Hz, with ICAS patients showing stronger inter-

hemispheric asymmetry compared to healthy controls (**Fig. 1K**), supporting a frequency-specific disruption of functional coherence in ICAS. We further conducted a group-level analysis of inter-hemispheric coherence across the infra-slow oscillatory frequency range (0.01-0.1 Hz, referred to as <0.1 Hz) in healthy controls and patients with unilateral ICAS. To compare coherence between groups, coherence values were Fisher Z-transformed to approximate a normal distribution, and Fisher Z-transformed coherence coefficients were computed between homotopic ROI pairs. As shown in **Fig. 1L**, group-averaged spectral coherence analysis revealed prominently reduced coherence values in the ICAS group, specifically in the 0.08-0.1 Hz range (~0.1 Hz), while both groups exhibited similar coherence patterns in the ultra-slow oscillatory frequency band (0.01-0.05 Hz). Statistical analyses confirmed that homotopic coherence was significantly lower in patients with ICAS than in healthy controls in the 0.08-0.1 Hz band (highlighted by a blue box in **Fig. 1M**). Similarly, heterotopic coherence analysis also showed a significant group difference at 0.08-0.1 Hz (**Fig. 1N**).

In summary, supporting our first hypothesis, these findings indicate that the disruption of inter-hemispheric coherence in patients with ICAS is frequency-specific, centered around ~0.1 Hz, corresponding to the known range of vasomotor activity (5). Moreover, the results clearly distinguish spectral coherence FC at ~0.1 Hz between ICAS patients and healthy controls.

Brain-wide mapping of inter-hemispheric coherence across canonical rs-fMRI networks in ultra-slow (<0.05 Hz) and slow (~0.1 Hz) oscillatory frequency bands

Based on the inter-hemispheric PSD and coherence analysis, we examined the frequency-dependent coherence across large-scale networks in healthy controls and patients with unilateral ICAS. To define inter-hemispheric rs-fMRI networks, we employed seven canonical rs-fMRI networks proposed by Yeo and colleagues (41). The seven rs-fMRI networks consisted of: Default Mode Network (DMN), Somatomotor Network (SMN), Dorsal Attention Network (DAN), Visual Network (VIN), Salience Network (SAN), Limbic Network (LIN), and Executive Control Network (ECN). In addition, the subcortical network (SubCort) was included in the analysis. Each AICHA ROI was assigned to one of these canonical rs-fMRI networks following the procedures described by Labache et al. (44) (**Fig. 2A** and **Table S1**). For network-level analysis of homotopic and heterotopic FC, we first visualized coherence matrices across the Yeo-defined networks for both groups at full infra-slow oscillatory frequency band (0.01-0.1 Hz). Interestingly, lower coherence values were observed in the ICAS group for heterotopic ROI pairs, particularly across VIN, SMN, and DAN (**Fig. 2B**). To examine frequency-specific patterns, we re-calculated inter-hemispheric coherence matrices at two distinct frequency bands: <0.05 Hz and ~0.1 Hz. This analysis revealed notably diminished homotopic and heterotopic coherence across all networks in the ICAS group at ~0.1 Hz, while coherence pattens at ultra-slow oscillatory frequency band (<0.05 Hz) remained largely comparable between the two groups (**Fig. 2C** and **E**).

To reduce noise and thus more clearly compare the coherence patterns across networks between the two groups, the ROI-based inter-hemispheric coherence matrices were averaged within each of the predefined networks (**Fig. 2D** and **2F**). At <0.05 Hz, both groups exhibited similar inter-hemispheric coherence patterns, with strong coherence observed along homotopic network pairs (diagonal) and across heterotopic connections involving the VIN, SMN, DAN, and SAN (upper four networks in the off-diagonal) (**Fig. 2D** and **S1 A**). No significant differences in inter-hemispheric coherence were observed between the two groups in this frequency band (**Fig. 2G**). In contrast, at ~0.1 Hz, distinct coherence patterns emerged between the

two groups and the ICAS group displayed globally reduced inter-hemispheric coherence, both in homotopic (diagonal) and heterotopic (off-diagonal) networks (**Fig. 2F and S1 B**). Statistically significant reductions in coherence were found in the VIN, SMN, DAN, and ECN in patients with ICAS, suggesting these cortical regions may share common cerebrovascular mechanisms (43) (**Fig. 2H**).

In summary, supporting our second hypothesis regarding spatially organized functional networks, these results demonstrate that frequency-specific disruptions in inter-hemispheric coherence at ~0.1 Hz are consistently observed across the large-scale intrinsic brain networks. Moreover, the network-level coherence alterations at ~0.1 Hz can clearly be distinguished from those at <0.05 Hz (ultra-slow oscillatory frequency band), highlighting the functional significance of frequency-dependent FC alteration in patients with ICAS.

Regional vulnerability of inter-hemispheric BOLD coherence and vascular impairment inside watershed areas in patients with ICAS

To further explore regional effects on inter-hemispheric coherence, we investigated the impact of distinct perfusion conditions, i.e., inside vs. outside watershed areas, on frequency-dependent inter-hemispheric coherence in both healthy controls and patients with unilateral ICAS. As illustrated in **Fig. 3A**, we identified ROIs overlapping with pre-defined watershed areas using the AICHA atlas (42) (n = 41 ROIs, details in the **Methods**). These ROIs were used to assess frequency-dependent inter-hemispheric coherence and to evaluate regional quantitative hemodynamic MRI parameters such CBV, CBF, $CMRO_2$ and BOLD time lag (**Fig. 3A**). As shown in **Fig. 3B**, we quantified the distribution of the canonical rs-fMRI networks within the watershed areas: VIN: 54.3%, SMN: 4.8%, DAN: 15.8%, SAN: 0.0%, LIN: 22.2%, ECN: 38.9%, DMN: 10.0%, and SubCort: 13.6%. Notably, no ROI from SAN overlapped with the watershed area (**Table S2**).

To characterize spectral dynamics inside and outside watershed areas (**Table S2-3**), we computed group-averaged inter-hemispheric PSD differences ($|\Sigma(\Delta_{LR}\ PSD)|$) at the two distinct frequency bands (ultra-slow; <0.5 Hz and slow; ~0.1 Hz) for healthy controls and patients with ICAS. Notably, inside watershed areas, a significant group difference was observed only at ~0.1 Hz, whereas no significant differences were found at <0.05 Hz inside the watershed area, nor at either frequency band outside the watershed area (**Fig. 3C**). We also assessed group-averaged inter-hemispheric coherence in the same two frequency bands, again separately for regions inside and outside watershed areas. Consistent with the PSD results, significant group differences in both homotopic and heterotopic coherences were observed only at ~0.1 Hz inside the watershed area. In contrast, coherence values at ~0.1 Hz outside watershed areas, as well as at <0.05 Hz both inside and outside the watershed areas, did not differ significantly between the two groups (**Fig. 3D**, **S2**, and **S3**).

To further examine regional differences in inter-hemispheric coherence, we mapped coherence matrices across the canonical rs-fMRI networks separately for regions inside and outside watershed areas. For the two groups, network-averaged coherence matrices were computed at the two distinct frequency bands (<0.05 Hz and ~0.1 Hz). As shown in **Fig. 3E**, inside the watershed areas, overall coherence values at ~0.1 Hz were markedly diminished and spatially heterogeneous across the networks (with the exception of the SAN, which contained no ROI). The SubCort network exhibited low homotopic (diagonal) and heterotopic (off-diagonal) coherence values. These reductions are also visualized in the circular diagram, which illustrates pronounced decreases in inter-hemispheric coherence inside the watershed areas. Statistically, significantly lower coherence coefficients were observed in patients with ICAS across the seven cortical

networks (except DAN and SAN; SAN was not assigned) at ~0.1 Hz (**Fig. 3G**), underscoring the impact of regional perfusion impairment on frequency-specific inter-hemispheric FC. In contrast, outside the watershed areas (**Fig. 3F**), coherence values at ~0.1 Hz were only moderately reduced and were more homogeneous across heterotopic connections, while homotopic coherence remained relatively strong across most networks. The corresponding circular diagram confirms a lower degree of coherence reduction outside watershed areas compared to inside watershed areas. Only two networks, i.e., SMN and DAN, showed significantly lower inter-hemispheric coherence in patients with ICAS outside the watershed area (**Fig. 3H**).

In addition, to investigate the impact of distinct perfusion territories (i.e., inside vs. outside watershed areas) on multi-parametric quantitative hemodynamic MRI parameters, we first estimated relative CBV, CBF, relative $CMRO_2$, and BOLD time lag maps in healthy controls and patients with unilateral ICAS (**Fig. S4**). For each parameter, absolute inter-hemispheric differences were calculated by summing the difference between left and right hemispheres across homotopic ROI pairs: $|\Sigma(\Delta_{LR}\ CBV)|$, $|\Sigma(\Delta_{LR}\ CBF)|$, $|\Sigma(\Delta_{LR}\ CMRO_2)|$, and $|\Sigma(\Delta_{LR}\ \text{BOLD lag})|$ (details in **Methods**). These metrics were then compared between the two groups, separately for inside and outside of watershed areas (**Fig. 3I-J**). Interestingly, the inter-hemispheric difference in relative CBV, $|\Sigma(\Delta_{LR}\ CBV)|$ showed a prominent and statistically significant group difference inside the watershed areas ($p < 0.01$), but not outside. In contrast, CBF differences were significant in both regions ($p < 0.05$), showing diminished perfusion in the hemisphere ipsilateral to the stenosis (**Fig. S4 B**), while relative $CMRO_2$ differences did not reach statistical significance in either region. This finding may indicate a generalized disruption of flow-metabolism coupling in patients, regardless of perfusion territory, consistent with previous findings(30). For BOLD time lag, a significant inter-hemispheric difference was observed only outside the watershed areas ($p < 0.05$), while no significant difference was found inside the watershed areas, possibly reflecting asymmetric blood arrival times: the hemisphere ipsilateral to the stenosis show delayed perfusion outside the watershed territory, whereas both hemispheres exhibited more symmetric prolonged arrival times within the watershed areas (**Fig. S4 D**).

Taken together, in support of our third hypothesis regarding regions of distinct perfusion alterations, these findings demonstrate that aberrant inter-hemispheric rs-fMRI coherence at ~0.1 Hz is localized specifically to vulnerable regions at the border of vascular territories, i.e., the watershed areas, that are particularly affected by hypoperfusion. Importantly, this ~0.1 Hz-specific disruption in coherence appears to be independent of canonical rs-fMRI network organization. Furthermore, the results highlight the vulnerability of the watershed areas (28) in patients with unilateral ICAS, which are closely associated with a lateralized increase in CBV.

DISCUSSION

Guided by our three hypotheses, i.e., frequency specificity, brain-wide effect, and regional vulnerability, this study demonstrates that frequency-specific alterations in inter-hemispheric PSD and coherence at ~0.1 Hz, where vasomotor activity may appear, distinguish patients with unilateral ICAS from healthy controls, despite preserved coherence at the ultra-slow oscillatory frequency band (<0.05 Hz). Using our integrated multi-modal rs-fMRI method, we demonstrate that inter-hemispheric coherence at ~0.1 Hz is disrupted across canonical intrinsic networks and exhibits pronounced reduction in watershed areas, i.e., regions with particular perfusion vulnerability (28), where inter-hemispheric coherence is prominently diminished and CBV lateralization is significant. These findings not only bridge a gap in understanding how ICAS impacts brain-wide frequency-specific coherence, particularly in perfusion-vulnerable territories (watershed areas),

but also highlight the potential of rs-fMRI coherence at ~0.1 Hz as a non-invasive biomarker for early cerebrovascular dysfunction.

Our multi-modal fMRI analysis reveals notably desynchronized time series, diminished coherence matrices, and lateralized PSDs at ~0.1 Hz in patients with unilateral ICAS, accompanied by impaired CBV inside watershed areas. While these findings provide indirect evidence for vasomotor dysfunction, the physiological interpretation of ~0.1 Hz oscillations requires caution, as such oscillations may also arise from Mayer waves, callosal projections, and other confounders (5, 6, 19) (**Fig. 4**). Vasomotor activity is central to regulating arterial reservoir volumes and maintaining the homeostasis of flow and pressure in vascular networks (1, 2). However, since BOLD fMRI signals predominantly reflect venous rather than arterial dynamics (34), interpreting vasomotion influences on BOLD coherence requires an appreciation of vessel-specific contributions (45). In particular, T2*-weighted EPI, commonly used for fMRI acquisition, is sensitive to large draining veins near superficial cortical layers. As a result, the slow fluctuations (~0.1 Hz) of resting-state fMRI signals may be largely confined to these superficial layers (18, 46-48). While arteries with smooth muscle cells generate vasomotor activity, capillaries (without muscle cells) lack such capability and only show passive responses due to homeostasis. Importantly, venules and veins also have smooth muscle cells (49) and can regulate vasomotor activity, supporting venous return (1, 3). In addition, prior studies have supported the existence of venous vasomotor activity (4, 50-53). Thus, as proposed by Mateo et al (5), impaired vasomotor oscillations may manifest in the BOLD fMRI signals as reduced inter-hemispheric coherence at ~0.1 Hz. Future studies are warranted to examine vessel-specific contributions to ~0.1 Hz oscillation.

While this study clearly identified frequency-specific coherence disruption at ~0.1 Hz, it remains an indirect measure of vasomotor activity. As inspired by Mateo et al (5) and illustrated in **Fig. 4**, several potential sources may influence signal fluctuations within this frequency range. First, Mayer waves, systemic oscillation in arterial blood pressure, may overlap at the same frequency range (~0.1 Hz) (19, 20). Since these oscillations can partially coincide with BOLD fluctuations, changes in cerebrovascular hemodynamics may influence the BOLD fMRI signals to some extent (9, 19, 54). Given that systolic and diastolic blood pressure did not differ significantly between healthy controls and ICAS patients (**Table S4**), systemic blood pressure differences are unlikely to account for the observed ~0.1 Hz oscillation in this study. However, Mayer waves reflect dynamic fluctuations rather than mean blood pressure; therefore, their potential contribution cannot be fully excluded, as blood pressure was not continuously monitored during fMRI scanning. Second, the corpus callosum, a major fibers bundle connecting homotopic brain regions, is thought to mediate inter-hemispheric FC (55-58). Diminished ~0.1 Hz oscillation observed in acallosal mice suggests disrupted callosal projections (5). The relative structural and functional contributions to ~0.1 Hz oscillations remain to be clarified in future studies (59, 60). Third, other confounders should also be taken into account. Although respiratory fluctuations (0.15-0.3 Hz) (61-64) were filtered out during pre-processing, cardiac pulsation (~1 Hz) could introduce aliasing artifacts near ~0.1 Hz, particularly given the Nyquist sampling limit of rs-fMRI signals (~0.4 Hz) (63-65). In addition, the bandpass filtering during preprocessing (0.01-0.1 Hz) may modulate the spectral profile near the upper boundary of this range. As demonstrated by He et al (66) and Choi et al (18), PSD analyses showed that spectral responses exhibit greater variability around ~0.1 Hz, following 1 over f power regime (18, 34, 46, 67, 68). Importantly, spectral peaks can also be influenced by frequency resolution and smoothing procedure applied during preprocessing (69-71). Sleep and fidgeting, both known to modulate vasomotor activity (6, 72-75), may have further contributed to variability at ~0.1 Hz, especially in this elderly cohort during relatively long

fMRI scanning. Therefore, future ICAS studies should address causality by comparing vasomotor activity between pre- and post-revascularization in ICAS patients (76) or by incorporating concurrent transcranial Doppler measurements to directly assess vasomotor activity alongside our multi-modal fMRI framework. In addition, animal models with experimentally induced ICAS (77) (see **Fig. S6**) could also provide direct evidence for the relationship between vasomotion impairments and inter-hemispheric coherence disruption when combined with concurrent optical recording.

Although vasomotor oscillations span a broad frequency range (0.01 to 0.3 Hz, centered near 0.1 Hz) (3, 6), respiratory aliasing artifacts often confound fMRI signals in the 0.15-0.3 Hz range in human fMRI (61-64), especially without concurrent respiratory recording or physiological noise correction. To minimize contamination from aliased respiratory signals and maximize physiological interpretability, we focused on slow fluctuations within the commonly used resting-state frequency band of 0.01-0.1 Hz (90), which are thought to include vasomotor activity. Specifically, we define the ~0.1 Hz band as the 0.08-0.1 Hz to probe vasomotor-related fluctuations, since spectral peaks of vasomotor activity in this range have been consistently observed in prior human studies using fMRI (11), near infrared spectroscopy (37), and multi-spectral optical intrinsic signal imaging (15).

In contrast to this clear FC disruption at ~0.1 Hz, ultra-slow oscillations (<0.05 Hz) remained stable in patients with ICAS (**Fig. 1L**, **2C-D**, and **2G**). This stable ultra-slow oscillations, together with preserved $CMRO_2$ (**Fig. 3I-J**), suggest preserved neuronal activity (34) and global arousal brain state via neuromodulators, such as adrenergic and cholinergic neurons (38, 78). This pattern followed a spatial gradient from strong to weak coherence, spanning from unimodal (VIN and SMN), multi-modal (DAN and SAN), to transmodal (ECN and DMN) networks, reflecting known functional hierarchies and principal gradient axes (38, 79). Moreover, the preserved ultra-slow oscillations align with previous laminar fMRI findings (18, 46), and differences in ultra-slow coherence between cortical and subcortical structures may reflect distinct neurovascular coupling mechanisms (**Fig. 2D**). However, since we did not directly measure neuronal activity, the interpretation of preserved $CMRO_2$ requires caution. In this study, $CMRO_2$ was estimated from relative oxygen extraction fraction (OEF; ≈ R2′/ CBV) and CBF, as described in the **Methods** (28) (**Fig. S4**). Thus, preserved $CMRO_2$ may reflect opposing changes of OEF and CBF in the hemisphere ipsilateral to ICAS. Although vasomotor oscillations can be closely coupled with neural activity, they can also occur independently as optogenetic manipulation has confirmed vasomotion is unidirectional (5). Concurrent neuronal recording combined with human fMRI would help clarify the relationship between neuronal activity, ultra-slow oscillations (<0.05 Hz), and slow oscillations (~0.1 Hz) as has been shown in animal studies (5, 16, 34).

Watershed regions are of particular clinical relevance in ICAS patients (28, 29, 39). Inside watershed areas, coherence matrices at ~0.1 Hz showed pronounced spatial heterogeneity across networks, consistent with the more severe hemodynamic impairments reported in prior work (28, 29) (**Fig. 3E**). This heterogeneity likely reflects an interplay between compensation mechanisms (e.g., collateralization and autoregulation) (80, 81) and impaired vasomotor control (1-3). In contrast, coherence at ~0.1 Hz outside watershed areas was spatially homogeneous and relatively preserved (**Fig. 3F**), although diminished coherence at ~0.1 Hz was observed in SMN and DAN outside watershed areas, potentially due to age-related limitations in compensatory capacity in ICAS patients (**Fig. 3H**). These observations suggest that ~0.1 Hz-related coherence could serve as a sensitive marker of regional vulnerability to vascular impairment in ICAS patients, highlighting the increased sensitivity inside watershed areas.

A major methodological strength of this study is the integration of frequency-specific rs-fMRI analysis with multi-parametric hemodynamic MRI, enabling the identification of vasomotion-related disruptions in functional dynamics and region-specific vascular vulnerabilities, particularly inside watershed areas. By examining PSD and coherence at two distinct frequency bands, i.e., ultra-slow (<0.05 Hz) and vasomotor (~0.1 Hz), and linking these metrics to quantitative maps of CBV, CBF, $CMRO_2$, and BOLD time lag, we demonstrated that inter-hemispheric desynchronization at ~0.1 Hz is specifically associated with ipsilaterally increased CBV, as a potential factor related to impaired vasomotion due to chronic vasodilation. In contrast, conventional correlation-based FC measures failed to detect significant group differences between healthy controls and ICAS patients (31, 32) (**Fig. S5**), due to their limited sensitivity to frequency-specific impacts on FC. Our multi-modal fMRI framework, therefore, extends beyond conventional correlation-based approaches, enabling the investigation of brain-wide, frequency-specific functional dynamics and vascular contributions to rs-fMRI signals in ICAS patients. In the future, coherence-based fMRI may offer valuable insights for detecting subtle vascular impairment and functional desynchronization in patients with neurological and neurovascular disorders, including but not limited to ICAS.

In conclusion, our study demonstrates that inter-hemispheric BOLD coherence at ~0.1 Hz may serve as a frequency-sensitive and spatially specific marker of cerebrovascular dysfunction in patients with unilateral ICAS. These findings help bridge the gap between vascular pathology and resting-state functional disruption, and highlight the potential of coherence-based spectral analysis as a non-invasive biomarker not only for ICAS but also for other clinical conditions associated with vasomotion impairments, including stroke, small vessel disease, dementia, and Alzheimer's Disease (21, 35, 82-84).

MATERIALS and METHODS

In this study, we analyzed a subsample of existing multi-modal MRI data from our previous study, from which different aspects have already been published (27-33).

SUBJECT DETAILS AND MULTI-MODAL MRI DATA ACQUISITION

Subjects

All participants provided written informed consent prior to scanning in accordance with the policies of the institution's Human Research Committee. The study was approved by the Institutional Review Board of the Klinikum rechts der Isar at Technical University of Munich. Patients with unilateral asymptomatic ICAS were recruited through the outpatient clinic for carotid stenoses at the Department of Vascular and Endovascular Surgery, while healthy control participants were recruited via word-of-mouth advertisement. As previously reported (27-33), the study enrolled 29 patients with high-grade, unilateral, asymptomatic ICAS (confirmed by duplex ultrasonography; all >70% stenosis based on NASCET criteria (85)) and 30 age-matched healthy controls. Each participant underwent a clinical assessment that included a medical history review, basic neurological and psychiatric screening, and an MRI scan. Patients were classified as clinically asymptomatic if they exhibited no neurological symptoms such as stroke, transient ischemic attack (TIA), or paresis. Individuals with a history of neurological or psychiatric disorders, clinically significant structural brain abnormalities, or MRI contraindications were excluded. Due to insufficient MRI data quality, two patients and four healthy controls were excluded from the analysis, resulting in a final sample of 27 patients (11 females; mean age 70.3 ± 7.2 years) and 26 healthy controls (15 females; mean

age 70.3 ± 4.8 years). Detailed demographic information was described in Supplementary Information (**Table S4**).

Multi-modal rs-fMRI and multiparametric quantitative MRI data acquisition

All MRI data were acquired on a whole-body 3T Ingenia MRI scanner (Philips Healthcare, Best, The Netherlands) equipped with a 16-channel (dynamic susceptibility contrast (DSC) MRI) or a 32-channel head coil (for others) (**Fig. 1A**). Detailed acquisition parameters are described in the Supplementary Information. In short: For assessing power spectral density (PSD), coherence of BOLD fMRI signal time series, T2*-weighted multiband echo planar imaging (EPI) data were acquired under resting-state conditions. The acquisition parameters were as follows: repetition time (TR) = 1200 ms, echo time (TE) = 30 ms, total acquisition time = 10 minutes, flip angle (FA) = 70°, multiband factor = 2, SENSE factor = 2, 38 slices, matrix size = 192x192, voxel size = 3x3x3 mm^3, and 500 dynamic scans. For the anatomical reference (**Fig. 1B**), T1-weighted magnetization prepared rapid gradient echo (MPRAGE) data were acquired with 170 sagittal slices (**Fig. 1C**).

Quantitative perfusion and oxygenation parameter were acquired and processed as described in detail previously (28, 30, 32). Relative CBV was derived from DSC MRI data following bolus injection of gadolinium-based contrast agent (Gd-Dota; concentration 0.5 mmol/ml, dose 0.1 mmol/kg, minimum 7.5 mmol per subject). CBF was measured using pseudo-continuous arterial spin labeling (pCASL) sequence in accordance with the ISMRM Perfusion Study Group consensus recommendations (86) using a prolonged post-labeling delay of 2000 ms and applying background suppression. The OEF was calculated from R2′ ($= 1/T2^* - 1/T2$) and CBV, where $T2^*$ and $T2$ were derived from separate GRE and GRASE sequences, respectively, according to the multiparametric quantitative BOLD approach (87). Relative $CMRO_2$ was then estimated from the product of relative OEF and CBF (88, 89).

DATA PROCESSING

All data processing was performed using MATLAB (Mathworks, Natick, MA, version R2023a), Python (version 3.9.13), and R (version 4.4.0). Detailed descriptions of the processing and analysis workflows have been published in previous studies (18, 31, 32, 46). All figures were generated using Python (version 3.9.13), R (version 4.4.0), and FreeSurfer (version 7.4.1).

DATA PROCESSING FOR BOLD-fMRI

BOLD signal processing

We analyzed a subsample of 53 participants—27 patients (11 female) and 26 healthy controls (15 females)—selected based on sufficient MRI for analysis (e.g., absence of motion artifacts and valid values in AICHA ROIs).

As described in previous works (31, 32), BOLD fMRI data were pre-processed using the Data Processing Assistant for Resting-State fMRI advanced edition (DPARSFA) toolbox V5.0_200401 (91) and SPM12 (v7771; Wellcome Trust Centre for Neuroimaging, UCL, London, UK) using MATLAB (R2019b; MathWorks, Natick, MA, USA). Pre-processing included discarding of the first ten EPI volumes to reach steady-state magnetization, spatial realignment of acquired EPI volumes, slice-timing correction, reorientation to the anterior-posterior commissure, nuisance covariate regression (six motion parameter and a linear trend), spatial smoothing with a 6 mm full width at half maximum kernel, and temporal bandpass

filtering (0.01 to 0.1 Hz). Anatomical images were first neck cropped and then co-registered with functional EPI images, followed by segmentation using Diffeomorphic Anatomical Registration Through Exponentiated Lie Algebra (DARTEL) (92).

For each individual subject, EPI fMRI data were parcellated using the AICHA (42) (**Fig. 1B**), which resulted in 192 pairs of homotopic ROIs, yielding a total of 384 cortical and subcortical gray matter ROIs (**Fig. 1C**).

BOLD time series were extracted from the 192 homotopic ROI pairs, and Z-score normalization was applied prior to power spectral density (PSD), coherence, and correlation analyses. Z-score normalization was computed as $z = (x - \mu)/\sigma$, where x represents the original fMRI time series and μ and σ denote its mean and the standard deviation, respectively (using the 'zscore' function in MATLAB). In representative cases—a healthy control and a patient with unilateral ICAS (**Fig. 1G-I**)—Z-score normalized fMRI time series were averaged across homotopic ROI pairs to illustrate differences in temporal patterns (**Fig. 1D** and **G**). To more specifically compare infra-slow oscillations (<0.1 Hz), representative Z-score normalized fMRI time series were also extracted from one homotopic ROI pair (precuneus) and one heterotopic ROI pair (precuneus and lingual gyrus) in both subjects (**Fig. 1H** and **I**).

PSD analysis

Z-score normalized fMRI time series were transformed into PSD values to assess amplitude differences in resting-state BOLD signal power between the two groups. For group analysis, PSDs of bilateral rs-fMRI signals were compared in the typical resting-state frequency band, i.e., 0.01-0.1 Hz (18, 31, 32, 34, 46, 90, 93) (**Fig. 1J**). To quantify inter-hemispheric differences, PSD differences between the left and right hemispheres were summed across all homotopic ROI pairs and converted to absolute values, $|\Sigma(\Delta_{LR}\ PSD)| = |\Sigma(PSD_{Left} - PSD_{Right}|$, at two distinct frequency bands; 0.01-0.05 Hz and 0.08-0.1 Hz (**Fig. 1K**). PSD estimation was performed using Welch's method ('pwelch' function in MATLAB) with a Hamming window length of 128, Fast Fourier transform (FFT) length of 100, and 50% overlap. The frequency resolution was 1/120 s = 0.0083 Hz. The two distinct frequency bands were 0.01-0.05 Hz (referred to as <0.05 Hz) and 0.08-0.1 Hz (referred to as ~0.1 Hz in the following).

Spectral coherence analysis

Coherence analysis was employed to investigate the spectral dynamics of inter-hemispheric FC, as coherence is widely regarded as a frequency-domain measure of FC (18, 34, 46, 94, 95). Higher coherence coefficients are generally interpreted as indicating stronger FC, whereas lower coefficients suggest reduced FC. In this study, spectral coherence was treated as a key marker for frequency-specific inter-hemispheric FC. To examine differences in coherence patterns between healthy controls and patients with unilateral ICAS, group-averaged spectral coherence was analyzed for both homotopic and heterotopic FC across the infra-slow oscillatory frequency range (<0.1 Hz), specifically focusing on two distinct frequency bands: <0.05 Hz and ~0.1 Hz. Z-score normalized fMRI time series were used for coherence calculations to eliminate potential bias stemming from the baseline signal intensity differences between two hemispheres. The coherence coefficient between two signals x and y—representing either homotopic or heterotopic ROI pairs—is defined as follows:

$$Coherence_{xy}(f) = \frac{\left|P_{xy}(f)\right|^2}{P_{xx}(f) * P_{yy}(f)}$$

where $P_{xx}(f)$ and $P_{yy}(f)$ denote the auto spectral densities of signals x and y, respectively, and $P_{xy}(f)$ is the cross-spectral density between them.

Coherence was computed using the magnitude-squared coherence estimate method ('mscohere' function in MATLAB, Mathworks, Natick, MA) with a hamming window length: 128, FFT length: 100, overlap: 50%). As in the PSD analysis, the frequency resolution was 1/120 s = 0.0083 Hz, allowing for the characterization of coherence patterns across the infra-slow oscillatory frequency range (<0.1 Hz). Two distinct frequency bands were examined: 0.01-0.05 Hz (referred to as <0.05 Hz) and 0.08-0.1 Hz (referred as to ~0.1 Hz). To facilitate group-level comparison, coherence coefficients between inter-hemispheric ROIs were Fisher Z-transformed prior to averaging within each frequency bands and group (96) (**Fig. 1L-N**).

Temporal correlation analysis

To complement the coherence analysis, temporal correlation analysis was conducted to assess inter-hemispheric FC across homotopic and heterotopic ROI pairs. As in the coherence analysis, Z-score normalized fMRI time series were used for both healthy controls and patients with unilateral ICAS.
The Pearson correlation coefficient between two signals x and y is defined as the following equation:

$$Correlation_{xy}(a,b) = \frac{\sum_{i=1}^{n}(x_{a,i} - \bar{x}_a)(y_{b,i} - \bar{y}_b)}{\sqrt{\sum_{i=1}^{n}(x_{a,i} - \bar{x}_a)^2 \sum_{i=1}^{n}(y_{b,i} - \bar{y}_b)^2}}$$

where x and y are the fMRI time series from ROIs a and b, respectively; i indicates the time points; and $\bar{x}_a$, $\bar{y}_b$ are the mean values of each time series.

Correlation coefficients were computed using 'corr' function in MATLAB (type: Pearson, rows: pairwise). As with coherence, Fisher-Z transform was applied to correlation values prior to averaging across inter-hemispheric ROI pairs within each group (**Fig. S5 A**).

Network-specific FC analysis

To assess the regional specificity of inter-hemispheric rs-fMRI, seven canonical rs-fMRI networks were utilized as defined by Yeo and colleagues (41). These networks were derived from a dataset of 1,000 healthy individuals scanned on 3T Tim Trio MRI scanners (Siemens, Erlangen, Germany), and are widely used to characterize large-scale distributed network organization in human fMRI research. The seven networks included: Default Mode Network (DMN), Somatomotor Network (SMN), Dorsal Attention Network (DAN), Visual Network (VIN), Salience Network (SAN), Limbic Network (LIN), and Executive Control Network (ECN). In addition, subcortical network (SubCort) was delineated.

For network-specific FC analysis, inter-hemispheric coherence matrices were computed using homotopic and heterotopic AICHA ROI pairs across the infra-slow oscillatory frequency band (0.01-0.1 Hz). Each AICHA ROI was assigned to one of the canonical rs-fMRI networks based on spatial overlap with the AICHA atlas (42) and Yeo's network parcellation (41), following procedures described by Labache et al. (44) (**Fig. 2A**). The coherence matrices were then reordered for each participant group (healthy controls and patients with unilateral ICAS) according to the canonical networks order: VIN, SMN, DAN, SAN, LIN, ECN, DMN, and SubCort. The reordered coherence matrices were averaged across three infra-slow frequency bands: the full infra-slow band (0.01-0.1 Hz; **Fig. 2B**), a ultra-slow oscillatory frequency band

(0.01-0.05 Hz; **Fig. 2C**), and a slow oscillatory frequency band (0.08-0.1 Hz; **Fig. 2E**). Fisher-Z transform was applied prior to averaging and inverted after averaging to ensure appropriate statistical treatments. To assess regional specificity of inter-hemispheric FC across the networks, coherence values were averaged within each network for the two distinct frequency bands (<0.05 Hz and ~0.1 Hz) (**Fig. 2D** and **F**). Detailed information on the mapping of AICHA ROIs to canonical networks is provided in the Supplementary **Table S1**).

Identification of distinct perfusion territory

In patients with ICAS, the most vulnerable brain regions are located in the watershed areas, as these regions are particularly susceptible to reductions in CBF. Watershed areas are located at the cortical border zones between major arterial territories—namely, of the anterior, middle, and posterior cerebral arteries (ACA, MCA, and PCA)—as well as at internal border zone between lateral lenticulo-striate arteries (LSA) and MCA (28, 39, 97) (**Fig. 3A**). Because these regions are furthest from primary arterial supply and depend on distal branches of the major arteries, watershed areas can be defined based on temporal perfusion delay (29).

In this study, individual watershed areas were identified using DSC MRI-derived time-to-peak (TTP) maps, following the method described by Kaczmarz and colleagues (28, 29). To alleviate variability in the definition and boundaries of watershed areas and to ensure spatial alignment with AICHA ROIs, a group-level watershed area mask was generated by averaging the individual masks across subjects (n = 52; one patient was excluded due to insufficient data quality) Based on the spatial overlap between the AICHA atlas and the group-defined watershed regions, AICHA ROIs were assigned to the watershed territory using a threshold of 95% overlap. A total of 41 ROI pairs, spanning canonical rs-fMRI networks and subcortical regions, were identified and confirmed though additional visual inspection. The watershed area mask was computed using visualization tools from Nilearn Python library (https://nilearn.github.io/dev/modules/plotting.html) and array transformation functions from Numpy Python library (https://numpy.org).

Spectral PSD and coherence analyses inside and outside watershed Areas.

To compare different spectral dynamics of PSDs and coherence inside versus outside the watershed areas, the absolute values of interhemispheric PSD differences were summed across homotopic ROI pairs located either inside or outside watershed areas. These summed differences, $|\Sigma(\Delta_{LR}\ \mathrm{PSD})|$, were computed separately for the two distinct frequency bands; 0.05 Hz and ~0.1 Hz. The resulting values were then compared between the two groups (**Fig. 3C**). Similarly, coherence values between homotopic or heterotopic ROI pairs were calculated separately for inside and outside the watershed area. Fisher Z-transform was applied prior to averaging, and inverse Fisher Z-transform was applied after averaging coherence values across ROI pairs, separately for the two distinct frequency bands in each group (**Fig. 3D**, **S2 A**, and **S3 A**).

For network-specific analyses of FC inside and outside watershed areas, AICHA ROIs overlapping with the defined watershed territory were reordered according to the canonical rs-fMRI networks and subcortical regions. Network-specific coherence matrices were then averaged across the two distinct frequency bands (<0.05 Hz and ~0.1 Hz), separately for regions inside and outside the watershed areas in each group. Fisher Z-transformation was applied prior to averaging coherence values across the networks, and inverse Z-transformation was performed after averaging. To visualize network-specific FC, circular diagrams were

generated to represent the strength of coherence between the eight brain networks—comprising the seven canonical rs-fMRI networks and the subcortical network. Visualization was performed in R using 'ggraph' R library (package version 2.2.1). Detailed information on the AICHA ROIs overlapping with the distinct perfusion territories (i.e., inside vs. outside watershed areas) is provided in the Supplementary Information (**Table S2-3**).

DATA PROCESSING FOR MULTIPARAMETRIC QUANTITATIVE MRI

Estimation of CBV, CBF, $CMRO_2$ and BOLD time lag in Gray Matter

Hemodynamic MRI parameter maps, i.e., relative CBV (from the DSC MRI), and CBF (from pCASL MRI), and relative OEF ≈ R2′/ CBV were calculated as described previously (28) (**Fig. S4**). Subsequently, relative $CMRO_2$ maps were estimated using the following equation:

$$CMRO_2 = C_a \times Y_a \times OEF \times CBF$$

where C_a is the oxygen carrying capacity of arterial blood (μmol O_2 per 100 ml blood) and Y_a is the hemoglobin oxygen saturation level of arterial blood. Following the work reported by An and colleagues (98), we assumed that $Y_a \approx 1$ and $C_a = 0.19$ to simplify the estimation. To assess inter-hemispheric difference in BOLD time lag, lag time maps were generated from BOLD fMRI data using cross-correlation analysis in both groups. For each AICHA ROI, lag times were calculated as the time shift (ranging from -20 to +20 TRs) that maximized the cross-correlation coefficient with the fMRI signal from superior sagittal sinus. This analysis was implemented using the Python toolbox 'rapiditide', as described previously (32). Detailed signal processing steps were provided in previous works (31, 32).

Inter-hemispheric differences in multiparametric quantitative MRI

To assess individual MRI parameter maps (CBV, CBF, $CMRO_2$, and BOLD time lag), individual parameter maps were first parcellated using the AICHA atlas (42). To compare differences between homotopic ROI pairs located inside versus outside the watershed areas, absolute inter-hemispheric differences were computed for each parameter. Specifically, for each subject, the absolute differences between left and right hemispheres were summed across homotopic ROI pairs using the following equation: $|\Sigma(\Delta_{LR}\ \text{MRI Parameter})| = |\Sigma(\text{MRI Parameter}_{Left} - \text{MRI Parameter}_{Right}|$. This calculation was performed separately for ROIs inside and outside the watershed areas (**Fig. 3I-J**).

STASTICAL ANALYSIS

To assess group differences in PSD and coherence, two-sample t-tests were performed to compare the mean values between healthy controls and patients with unilateral ICAS, considering p-values < 0.05 or < 0.01 statistically significant. For coherence analysis, Fisher-Z transform was applied to the coherence coefficient prior to the t-test to satisfy the model assumption (i.e., normal distribution). For comparison of inter-hemispheric differences in quantitative hemodynamic MRI parameters (CBV, CBF, $CMRO_2$, and BOLD time lag), Wilcoxon rank-sum tests were used to evaluate differences between the two groups separately for inside and outside of watershed, using the same significant thresholds (p-values < 0.05 or < 0.01).

Data availability

Availability of human subject data is restricted due to data privacy regulations. Data sharing requires specific ethics votes and data transfer agreements. Processed non-image data generated during this study are available from the corresponding author upon reasonable request.

Code availability

The related image processing codes are available from the corresponding author upon reasonable request.

Acknowledgements

We thank Jacob Duckworth, Drs. David Kleinfeld, Filip Sobczak, Loïc Labache, and Afra Wohlschläger for their helpful comments and discussions. We also thank Yehwan (Issac) Choi for his schematic illustrations. This work was supported the Deutsche Forschungsgemeinschaft (DFG, German Research Foundation) – project number 395030489 and ev. Studienwerk Villigst (personal grant to Gabriel Hoffmann).

Author contributions

C.P. and C.S. designed and supervised the research, S.K. and C.P. performed experiments and acquired data, S.C. analyzed data, G.H., and S.S. provided technical support, S.C., X.Y., C.S., and C.P. wrote the manuscript.

Competing interests

S.K. is an employee of Philips GmbH Market DACH, Hamburg, Germany. X.Y. is a co-founder of MRIBOT LLC. The remaining authors declare no conflict of interest.

Additional information

Supplementary material for this paper can be found at the journal website.

REFERENCES

1. P. A. Nicoll, R. L. Webb, Vascular patterns and active vasomotion as determiners of flow through minute vessels. *Angiology* **6**, 291-308 (1955).
2. M. Intaglietta, Vasomotion and flowmotion: physiological mechanisms and clinical evidence. *Vascular Medicine Review* **1(2)**, 101-112 (1990).
3. C. Aalkjær, D. Boedtkjer, V. Matchkov, Vasomotion - what is currently thought? *Acta Physiol* **202**, 253-269 (2011).
4. Y. Wang, D. Hu, Y. Liu, M. Li, Cerebral artery-vein separation using 0.1-Hz oscillation in dual-wavelength optical imaging. *IEEE Trans Med Imaging* **30**, 2030-2043 (2011).
5. C. Mateo, P. M. Knutsen, P. S. Tsai, A. Y. Shih, D. Kleinfeld, Entrainment of Arteriole Vasomotor Fluctuations by Neural Activity Is a Basis of Blood-Oxygenation-Level-Dependent "Resting-State" Connectivity. *Neuron* **96**, 936-948 e933 (2017).
6. P. J. Drew, C. Mateo, K. L. Turner, X. Yu, D. Kleinfeld, Ultra-slow Oscillations in fMRI and Resting-State Connectivity: Neuronal and Vascular Contributions and Technical Confounds. *Neuron* **107**, 782-804 (2020).

7. B. R. Rosenblum, R. F. Bonner, E. H. Oldfield, Intraoperative measurement of cortical blood flow adjacent to cerebral AVM using laser Doppler velocimetry. *J Neurosurg* **66**, 396-399 (1987).
8. H. Seifert, K. Jager, A. Bollinger, Analysis of flow motion by the laser Doppler technique in patients with peripheral arterial occlusive disease. *Int J Microcirc Clin Exp* **7**, 223-236 (1988).
9. A. G. Hudetz, R. J. Roman, D. R. Harder, Spontaneous flow oscillations in the cerebral cortex during acute changes in mean arterial pressure. *J Cereb Blood Flow Metab* **12**, 491-499 (1992).
10. J. E. Mayhew *et al.*, Cerebral vasomotion: a 0.1-Hz oscillation in reflected light imaging of neural activity. *Neuroimage* **4**, 183-193 (1996).
11. P. P. Mitra, S. Ogawa, X. Hu, K. Ugurbil, The nature of spatiotemporal changes in cerebral hemodynamics as manifested in functional magnetic resonance imaging. *Magn Reson Med* **37**, 511-518 (1997).
12. D. Kleinfeld, P. P. Mitra, F. Helmchen, W. Denk, Fluctuations and stimulus-induced changes in blood flow observed in individual capillaries in layers 2 through 4 of rat neocortex. *Proc Natl Acad Sci U S A* **95**, 15741-15746 (1998).
13. H. Obrig *et al.*, Spontaneous low frequency oscillations of cerebral hemodynamics and metabolism in human adults. *Neuroimage* **12**, 623-639 (2000).
14. M. Razavi *et al.*, Source of low-frequency fluctuations in functional MRI signal. *J Magn Reson Imaging* **27**, 891-897 (2008).
15. A. Rayshubskiy *et al.*, Direct, intraoperative observation of ~0.1 Hz hemodynamic oscillations in awake human cortex: implications for fMRI. *Neuroimage* **87**, 323-331 (2014).
16. T. Broggini *et al.*, Long-wavelength traveling waves of vasomotion modulate the perfusion of cortex. *Neuron* **112**, 2349-2367 e2348 (2024).
17. K. A. Williams *et al.*, Comparison of alpha-chloralose, medetomidine and isoflurane anesthesia for functional connectivity mapping in the rat. *Magn Reson Imaging* **28**, 995-1003 (2010).
18. S. Choi, Y. Chen, H. Zeng, B. Biswal, X. Yu, Identifying the distinct spectral dynamics of laminar-specific interhemispheric connectivity with bilateral line-scanning fMRI. *J Cereb Blood Flow Metab* **43**, 1115-1129 (2023).
19. C. Julien, The enigma of Mayer waves: Facts and models. *Cardiovasc Res* **70**, 12-21 (2006).
20. M. Elstad, L. Walloe, K. H. Chon, K. Toska, Low-frequency fluctuations in heart rate, cardiac output and mean arterial pressure in humans: what are the physiological relationships? *J Hypertens* **29**, 1327-1336 (2011).
21. Y. Y. Zhang *et al.*, High-resolution vasomotion analysis reveals novel arteriole physiological features and progressive modulation of cerebral vascular networks by stroke. *J Cereb Blood Flow Metab* **44**, 1330-1348 (2024).
22. M. Silvestrini, E. Troisi, M. Matteis, L. M. Cupini, C. Caltagirone, Transcranial Doppler assessment of cerebrovascular reactivity in symptomatic and asymptomatic severe carotid stenosis. *Stroke* **27**, 1970-1973 (1996).
23. A. Gur, I. Bova, N. Bornstein, Is impaired cerebral vasomotor reactivity a predictive factor of stroke in asymptomatic patients? *Stroke* **27(12)**, 2188-2190 (1996).
24. M. Silvestrini *et al.*, Impaired cerebral vasoreactivity and risk of stroke in patients with asymptomatic carotid artery stenosis. *JAMA* **283**, 2122-2127 (2000).
25. A. Y. Gur, N. M. Bornstein, Cerebral vasomotor reactivity of bilateral severe carotid stenosis: is stroke unavoidable? *Eur J Neurol* **13**, 183-186 (2006).
26. K. Avirame *et al.*, Cerebral autoregulation and brain networks in occlusive processes of the internal carotid artery. *J Cereb Blood Flow Metab* **35**, 240-247 (2015).
27. C. Gleissner *et al.*, Hemodynamic MRI parameters to predict asymptomatic unilateral carotid artery stenosis with random forest machine learning. *Front Neuroimaging* **1**, 1056503 (2022).

28. S. Kaczmarz *et al.*, Hemodynamic impairments within individual watershed areas in asymptomatic carotid artery stenosis by multimodal MRI. *J Cereb Blood Flow Metab* **41**, 380-396 (2021).
29. S. Kaczmarz *et al.*, Increased variability of watershed areas in patients with high-grade carotid stenosis. *Neuroradiology* **60**, 311-323 (2018).
30. J. Gottler *et al.*, Flow-metabolism uncoupling in patients with asymptomatic unilateral carotid artery stenosis assessed by multi-modal magnetic resonance imaging. *J Cereb Blood Flow Metab* **39**, 2132-2143 (2019).
31. S. C. Schneider *et al.*, Resting-state BOLD functional connectivity depends on the heterogeneity of capillary transit times in the human brain A combined lesion and simulation study about the influence of blood flow response timing. *Neuroimage* **255**, 119208 (2022).
32. S. Schneider *et al.*, Stronger influence of systemic than local hemodynamic-vascular factors on resting-state BOLD functional connectivity. *Neuroimage* **281** (2023).
33. J. Gottler *et al.*, The stronger one-sided relative hypoperfusion, the more pronounced ipsilateral spatial attentional bias in patients with asymptomatic carotid stenosis. *J Cereb Blood Flow Metab* **40**, 314-327 (2020).
34. Y. He *et al.*, Ultra-Slow Single-Vessel BOLD and CBV-Based fMRI Spatiotemporal Dynamics and Their Correlation with Neuronal Intracellular Calcium Signals. *Neuron* **97**, 925-939 e925 (2018).
35. S. Holstein-Ronsbo *et al.*, Glymphatic influx and clearance are accelerated by neurovascular coupling. *Nat Neurosci* **26**, 1042-1053 (2023).
36. K. Kilic, A. Devor, The stop and go of glymphatic flow. *Nat Neurosci* **26**, 924-925 (2023).
37. H. Obrig *et al.*, Spontaneous low frequency oscillations of cerebral hemodynamics and metabolism in human adults. *Neuroimage* **12**, 623-639 (2000).
38. R. V. Raut *et al.*, Global waves synchronize the brain's functional systems with fluctuating arousal. *Sci Adv* **7** (2021).
39. A. Torvik, The pathogenesis of watershed infarcts in the brain. *Stroke* **15**, 221-223 (1984).
40. D. Bilecen *et al.*, fMRI of the auditory cortex in patients with unilateral carotid artery steno-occlusive disease. *J Magn Reson Imaging* **15**, 621-627 (2002).
41. B. T. Yeo *et al.*, The organization of the human cerebral cortex estimated by intrinsic functional connectivity. *J Neurophysiol* **106**, 1125-1165 (2011).
42. M. Joliot *et al.*, AICHA: An atlas of intrinsic connectivity of homotopic areas. *J Neurosci Methods* **254**, 46-59 (2015).
43. V. Kiviniemi *et al.*, Slow vasomotor fluctuation in fMRI of anesthetized child brain. *Magn Reson Med* **44**, 373-378 (2000).
44. L. Labache, T. Ge, B. T. T. Yeo, A. J. Holmes, Language network lateralization is reflected throughout the macroscale functional organization of cortex. *Nat Commun* **14**, 3405 (2023).
45. S. G. Kim, S. Ogawa, Biophysical and physiological origins of blood oxygenation level-dependent fMRI signals. *J Cereb Blood Flow Metab* **32**, 1188-1206 (2012).
46. S. Choi *et al.*, Laminar-specific functional connectivity mapping with multi-slice line-scanning fMRI. *Cereb Cortex* **32**, 4492-4501 (2022).
47. S. Choi *et al.*, Alpha-180 spin-echo-based line-scanning method for high-resolution laminar-specific fMRI in animals. *Imaging Neurosci (Camb)* **2** (2024).
48. Y. Tong, B. Frederick, Concurrent fNIRS and fMRI processing allows independent visualization of the propagation of pressure waves and bulk blood flow in the cerebral vasculature. *Neuroimage* **61**, 1419-1427 (2012).
49. F. X. Boittin, N. Macrez, G. Halet, J. Mironneau, Boittin FX, Macrez N, Halet G, Mironneau J. Norepinephrine-induced Ca(2+) waves depend on InsP(3) and ryanodine receptor activation in vascular myocytes. *American Physiological Society* **277**, 139-151 (1999).

50. T. W. Jones, Discovery that the veins of the bat's wing are endowed with rhythmical contractility and that onward flow of blood is accelerated by each contraction. *Philosophical Transactions of the Royal Society of London* **142**, 131-136 (1852).
51. M. P. Wiedeman, Effect of venous flow on frequency of venous vasomotion in the bat wing. *Circ Res* **5**, 641-644 (1957).
52. F. Gotoh *et al.*, Rhythmic changes in diameter of pial vessels and function of autonomic nervous system. *Cerebral Blood Flow: Effects of Nerves and Neuro-transmitters, edited by Heistad DD. Amsterdam: Elsevier North Holland*, 409-417 (1982).
53. W. G. Hundley, G. J. Renaldo, J. E. Levasseur, H. A. Kontos, Vasomotion in cerebral microcirculation of awake rabbits. *Am J Physiol* **254**, H67-71 (1988).
54. J. R. Bumstead, A. Q. Bauer, P. W. Wright, J. P. Culver, Cerebral functional connectivity and Mayer waves in mice: Phenomena and separability. *J Cereb Blood Flow Metab* **37**, 471-484 (2017).
55. M. H. Mohajerani, D. A. McVea, M. Fingas, T. H. Murphy, Mirrored bilateral slow-wave cortical activity within local circuits revealed by fast bihemispheric voltage-sensitive dye imaging in anesthetized and awake mice. *J Neurosci* **30**, 3745-3751 (2010).
56. M. E. Magnuson, G. J. Thompson, W. J. Pan, S. D. Keilholz, Effects of severing the corpus callosum on electrical and BOLD functional connectivity and spontaneous dynamic activity in the rat brain. *Brain Connect* **4**, 15-29 (2014).
57. J. M. Johnston *et al.*, Loss of resting interhemispheric functional connectivity after complete section of the corpus callosum. *J Neurosci* **28**, 6453-6458 (2008).
58. M. Quigley *et al.*, Role of the corpus callosum in functional connectivity. *AJNR Am J Neuroradiol* **24**, 208-212 (2003).
59. L. Schmitzer *et al.*, Macro- and microvascular contributions to cerebral structural alterations in patients with asymptomatic carotid artery stenosis. *J Cereb Blood Flow Metab* **44**, 1629-1642 (2024).
60. A. Avena-Koenigsberger, B. Misic, O. Sporns, Communication dynamics in complex brain networks. *Nat Rev Neurosci* **19**, 17-33 (2017).
61. G. H. Glover, T. Q. Li, D. Ress, Image-based method for retrospective correction of physiological motion effects in fMRI: RETROICOR. *Magn Reson Med* **44**, 162-167 (2000).
62. R. M. Birn, K. Murphy, P. A. Bandettini, The effect of respiration variations on independent component analysis results of resting state functional connectivity. *Hum Brain Mapp* **29**, 740-750 (2008).
63. R. M. Birn, The role of physiological noise in resting-state functional connectivity. *Neuroimage* **62**, 864-870 (2012).
64. C. Caballero-Gaudes, R. C. Reynolds, Methods for cleaning the BOLD fMRI signal. *Neuroimage* **154**, 128-149 (2017).
65. C. Chang, J. P. Cunningham, G. H. Glover, Influence of heart rate on the BOLD signal: the cardiac response function. *Neuroimage* **44**, 857-869 (2009).
66. B. J. He, J. M. Zempel, A. Z. Snyder, M. E. Raichle, The temporal structures and functional significance of scale-free brain activity. *Neuron* **66**, 353-369 (2010).
67. B. Biswal, F. Z. Yetkin, V. M. Haughton, J. S. Hyde, Functional connectivity in the motor cortex of resting human brain using echo-planar MRI. *Magn Reson Med* **34**, 537-541 (1995).
68. B. J. He, Scale-free brain activity: past, present, and future. *Trends Cogn Sci* **18**, 480-487 (2014).
69. J. Muthuswamy, N. V. Thakor, Spectral analysis methods for neurological signals. *J Neurosci Methods* **83**, 1-14 (1998).
70. M. K. van Vugt, P. B. Sederberg, M. J. Kahana, Comparison of spectral analysis methods for characterizing brain oscillations. *J Neurosci Methods* **162**, 49-63 (2007).

71. D. Kleinfeld, P. P. Mitra, Spectral methods for functional brain imaging. *Cold Spring Harb Protoc* **2014**, 248-262 (2014).
72. X. Lei, Y. Wang, H. Yuan, A. Chen, Brain scale-free properties in awake rest and NREM sleep: a simultaneous EEG/fMRI study. *Brain Topogr* **28**, 292-304 (2015).
73. H. Helakari *et al.*, Human NREM Sleep Promotes Brain-Wide Vasomotor and Respiratory Pulsations. *J Neurosci* **42**, 2503-2515 (2022).
74. N. E. Fultz *et al.*, Coupled electrophysiological, hemodynamic, and cerebrospinal fluid oscillations in human sleep. *Science* **366**, 628-631 (2019).
75. N. L. Hauglund *et al.*, Norepinephrine-mediated slow vasomotion drives glymphatic clearance during sleep. *Cell* **188**, 606-622 e617 (2025).
76. H. L. Cheng *et al.*, Impairments in cognitive function and brain connectivity in severe asymptomatic carotid stenosis. *Stroke* **43**, 2567-2573 (2012).
77. H. Ishikawa *et al.*, A brief overview of a mouse model of cerebral hypoperfusion by bilateral carotid artery stenosis. *J Cereb Blood Flow Metab* **43**, 18-36 (2023).
78. J. Reimer *et al.*, Pupil fluctuations track rapid changes in adrenergic and cholinergic activity in cortex. *Nat Commun* **7**, 13289 (2016).
79. D. S. Margulies *et al.*, Situating the default-mode network along a principal gradient of macroscale cortical organization. *Proc Natl Acad Sci U S A* **113**, 12574-12579 (2016).
80. L. Zarrinkoob *et al.*, Blood Flow Lateralization and Collateral Compensatory Mechanisms in Patients With Carotid Artery Stenosis. *Stroke* **50**, 1081-1088 (2019).
81. M. Reinhard *et al.*, Bilateral severe carotid artery stenosis or occlusion - cerebral autoregulation dynamics and collateral flow patterns. *Acta Neurochir (Wien)* **145**, 1053-1059; discussion 1059-1060 (2003).
82. S. J. van Veluw *et al.*, Vasomotion as a Driving Force for Paravascular Clearance in the Awake Mouse Brain. *Neuron* **105**, 549-561 e545 (2020).
83. J. M. Wardlaw, C. Smith, M. Dichgans, Small vessel disease: mechanisms and clinical implications. *Lancet Neurol* **18**, 684-696 (2019).
84. L. Y. Di Marco, E. Farkas, C. Martin, A. Venneri, A. F. Frangi, Is Vasomotion in Cerebral Arteries Impaired in Alzheimer's Disease? *J Alzheimers Dis* **46**, 35-53 (2015).
85. S. NASCET, North American Symptomatic Carotid Endarterectomy Trial. Methods, patient characteristics, and progress. *Stroke* **22**, 711-720 (1991).
86. D. C. Alsop *et al.*, Recommended implementation of arterial spin-labeled perfusion MRI for clinical applications: A consensus of the ISMRM perfusion study group and the European consortium for ASL in dementia. *Magn Reson Med* **73**, 102-116 (2015).
87. S. Kaczmarz, F. Hyder, C. Preibisch, Oxygen extraction fraction mapping with multi-parametric quantitative BOLD MRI: Reduced transverse relaxation bias using 3D-GraSE imaging. *Neuroimage* **220**, 117095 (2020).
88. Z. B. Rodgers, J. A. Detre, F. W. Wehrli, MRI-based methods for quantification of the cerebral metabolic rate of oxygen. *J Cereb Blood Flow Metab* **36**, 1165-1185 (2016).
89. E. Biondetti, J. Cho, H. Lee, Cerebral oxygen metabolism from MRI susceptibility. *Neuroimage* **276**, 120189 (2023).
90. M. D. Fox, M. E. Raichle, Spontaneous fluctuations in brain activity observed with functional magnetic resonance imaging. *Nat Rev Neurosci* **8**, 700-711 (2007).
91. Y. Chao-Gan, Z. Yu-Feng, DPARSF: A MATLAB Toolbox for "Pipeline" Data Analysis of Resting-State fMRI. *Front Syst Neurosci* **4**, 13 (2010).
92. J. Ashburner, A fast diffeomorphic image registration algorithm. *Neuroimage* **38**, 95-113 (2007).
93. D. Cordes *et al.*, Frequencies contributing to functional connectivity in the cerebral cortex in "resting-state" data. *AJNR Am J Neuroradiol* **22**, 1326-1333 (2001).

94. F. T. Sun, L. M. Miller, M. D'Esposito, Measuring interregional functional connectivity using coherence and partial coherence analyses of fMRI data. *Neuroimage* **21**, 647-658 (2004).
95. M. Yaesoubi, E. A. Allen, R. L. Miller, V. D. Calhoun, Dynamic coherence analysis of resting fMRI data to jointly capture state-based phase, frequency, and time-domain information. *Neuroimage* **120**, 133-142 (2015).
96. D. M. Corey, W. P. Dunlap, M. Burke, Averaging Correlations: Expected Values and Bias in Combined Pearson rs and Fisher's z Transformations. *The Journal of General Psychology* **125**, 245-261 (1998).
97. I. Momjian-Mayor, J. C. Baron, The pathophysiology of watershed infarction in internal carotid artery disease: review of cerebral perfusion studies. *Stroke* **36**, 567-577 (2005).
98. H. An, W. Lin, A. Celik, Y. Z. Lee, Quantitative measurements of cerebral metabolic rate of oxygen utilization using MRI: a volunteer study. *NMR Biomed* **14**, 441-447 (2001).

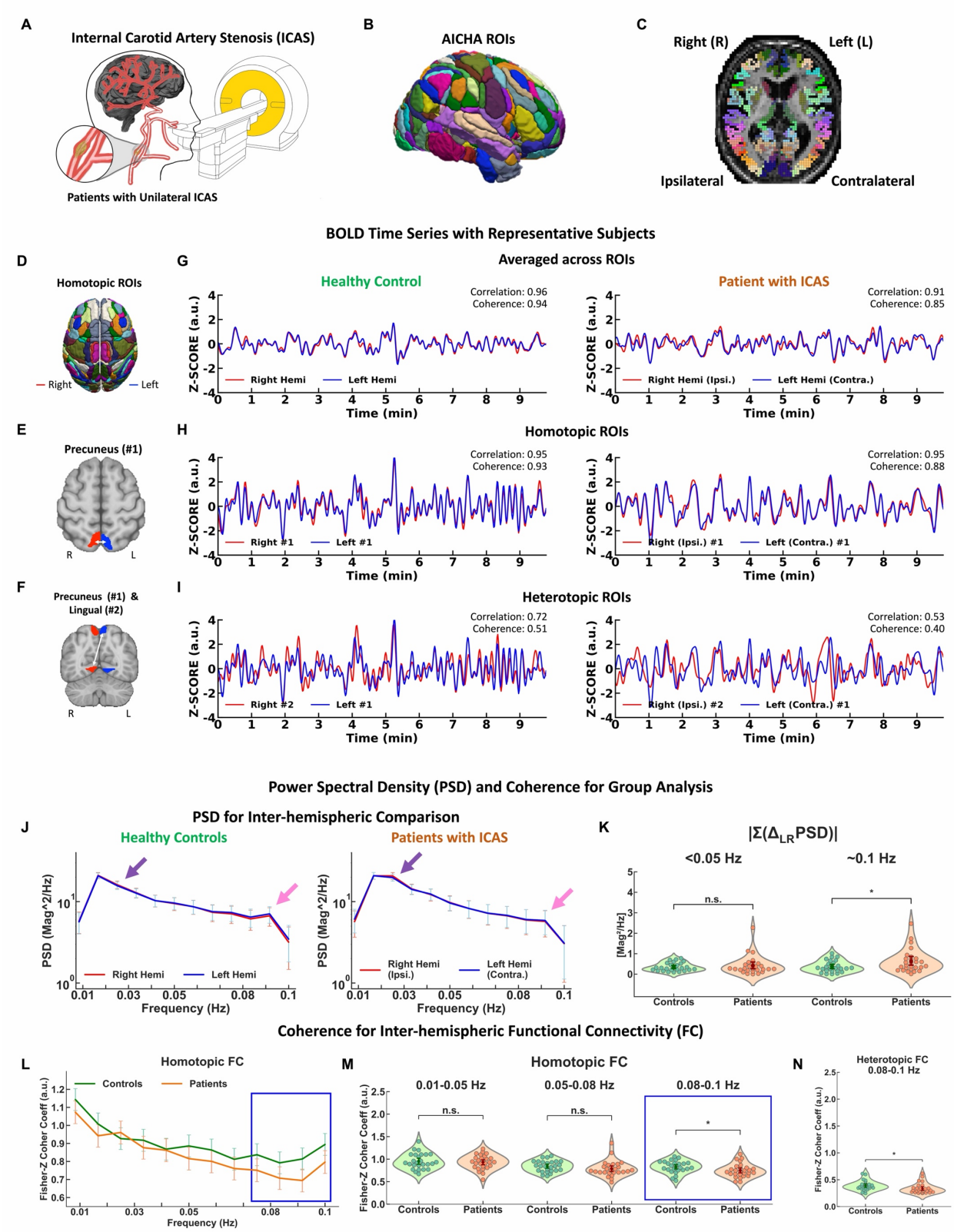

Figure 1. Frequency dependence of homotopic and heterotopic FC in healthy controls and patients with ICAS. A. Conceptual illustration of multi-modal MRI measurements in asymptomatic patients with

unilateral ICAS at 3T. **B.** Surface representation of AICHA brain parcellation (N = 384 ROIs). **C.** AICHA ROIs displayed on an axial T1-weighted MPRAGE image; identical colors indicate homotopic regions. **D-I**. BOLD time series for one representative subject from each group. **D.** illustration of homotopic ROI pairs defined by AICHA atlas. **E** and **F.** AICHA ROIs corresponding to a representative homotopic ROI pair (**E**; Precuneus) and a heterotopic ROI pair (**F**; Precuneus and Lingual). Red and blue indicate right and left hemispheric regions, respectively. **G.** Averaged Z-score normalized BOLD signal time series from right (red) and left (blue) hemispheres in a representative healthy control (left) and patient with ICAS (right). Correlation and coherence values are shown in each panel (top right). **H** and **I.** Z-score normalized BOLD time series from the homotopic (**H**) and heterotopic (**I**) ROI pairs for the same representative subjects as in panel **G**. Correlation and coherence values are shown in each panel. **J-N**. Power spectral density and coherence for group analysis. **J.** Group-averaged PSD curves of intra-hemispheric BOLD signals from healthy controls (left, n=26) and patients with ICAS (right, n=27). Error bars indicate mean ± SD across subjects. Purple and pink mark spectral peaks at ~0.02 Hz and ~0.1 Hz, respectively. **K.** Group-level absolute summed PSD differences between the left and right hemispheres, $|\Sigma(\Delta_{LR}\ \mathrm{PSD})|$ at <0.05 Hz and ~0.1 Hz (0.08-0.1 Hz, see **Methods**) for healthy controls (green) and patients with ICAS (orange). **L** and **M.** Coherence for inter-hemispheric FC (healthy controls: green, patients with ICAS: orange). **L.** Group-level inter-hemispheric coherence (homotopic FC) at the infra-slow frequency band (0.01-0.1 Hz). The blue box marks the frequency range of ~0.08-0.1 Hz. Error bars indicate mean ± SEM across subjects. **M.** Comparison of homotopic FC across three distinct frequency bands: 0.01-0.05 Hz, 0.05-0.08 Hz, and 0.08-0.1 Hz (highlighted by blue box). **N.** Heterotopic FC at ~0.08-0.1 Hz. Statistical significance based on two-sample t-tests (∗: p-value < 0.05; n.s.: not significant). Diamond markers and outlines represent group means and 95% confidence intervals, respectively.

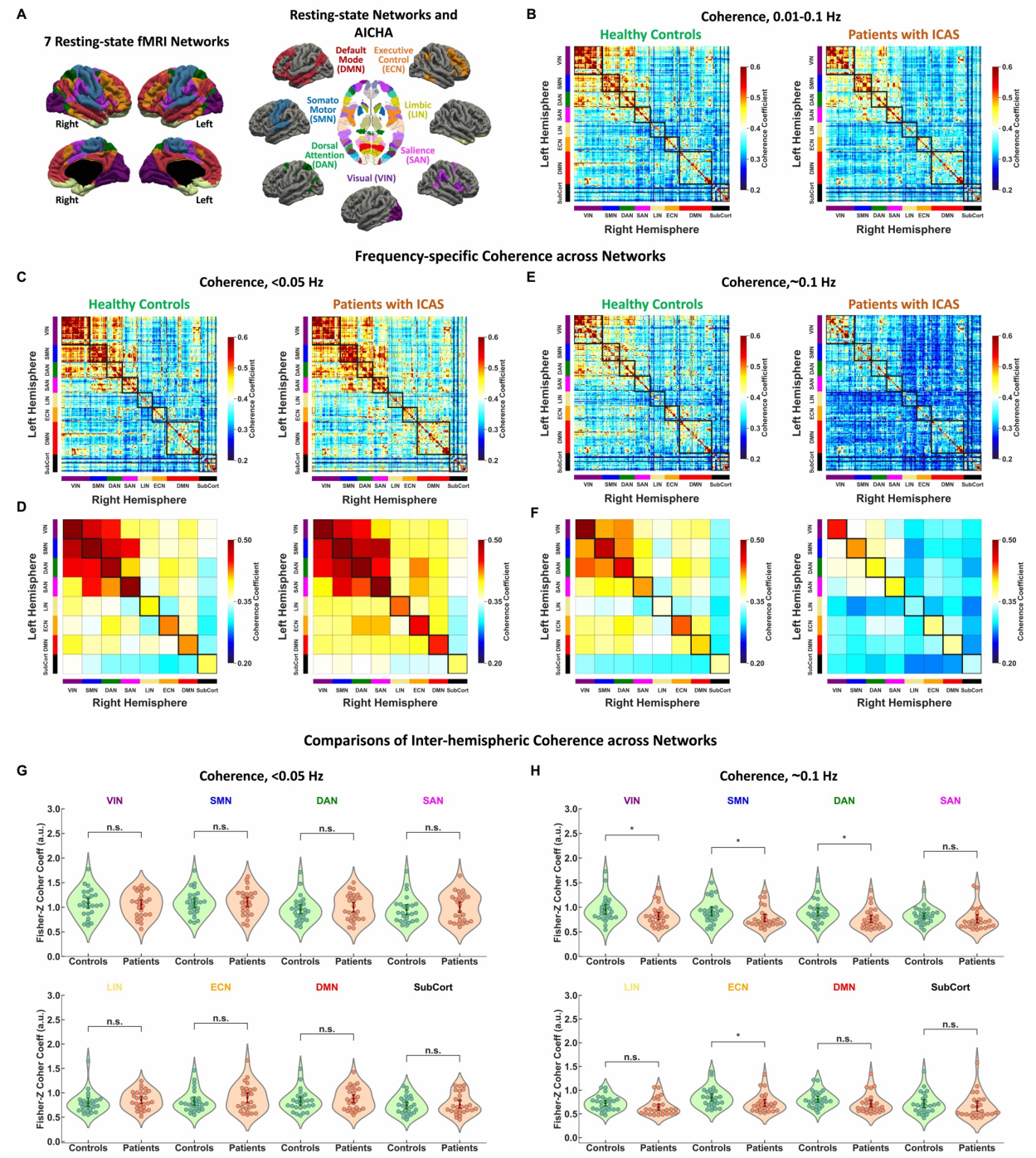

Figure 2. Frequency-dependent FC across networks in healthy controls and patients with ICAS. A. Surface representation of seven canonical rs-fMRI networks in right and left hemispheres (left), and their correspondence to AICHA ROIs (right). Overlapping AICHA ROIs were assigned to individual networks: Default Mode Network (DMN, red), Somatomotor Network (SMN, blue), Dorsal Attention Network (DAN, green), Visual Network (VIN, purple), Salience Network (SAN, magenta), Limbic Network (LIN, cream), and Executive Control Network (ECN, orange). The subcortical network (SubCort, black) was also

included. **B-F.** Inter-hemispheric coherence matrices of reordered AICHA ROIs across networks for healthy controls (left) and patients with ICAS (right). **B.** Coherence matrices for the full infra-slow frequency range (0.01-0.1 Hz). **C** and **D.** Frequency-specific coherence analysis at <0.05 Hz (0.01-0.05 Hz): **C.** Full network-level coherence matrices. **D.** Network-averaged coherence matrices across the eight networks. **E** and **F.** Frequency-specific coherence analysis at ~0.1 Hz (0.08-0.1 Hz): **E.** Full network-level coherence matrices. **F.** Network-averaged coherence. **G** and **H.** Group comparisons of inter-hemispheric coherence across networks between healthy controls (green) and patients with ICAS (orange): **G.** At <0.05 Hz. **H.** At ~0.1 Hz. Statistical comparisons were performed using two-sample *t*-tests (n.s.: no significance and ∗: p-value<0.05). Diamond markers and outlines represent group means and 95% confidence intervals.

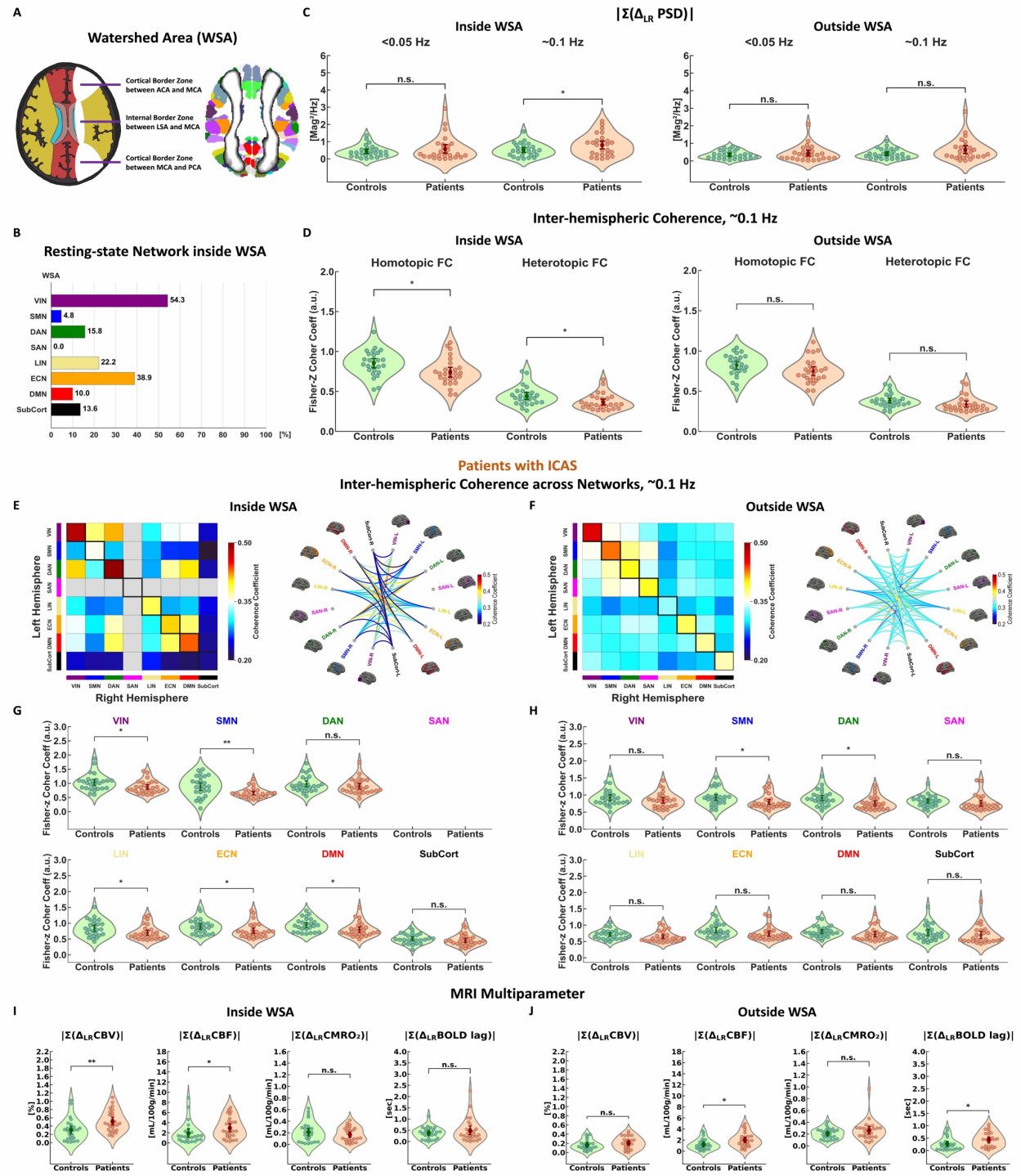

Figure 3. Frequency dependent FC inside and outside of watershed areas. A. Schematic illustration of watershed areas (WSAs, white), i.e., border zones: the cortical border zone between the anterior and middle cerebral arteries (ACA–MCA, top), the internal border zone between the lateral striate arteries (LSA) and MCA (middle), and the cortical border zone between the middle and posterior cerebral arteries (MCA–PCA, bottom). Right: Group-average bilateral WSA mask (white) from ICAS patients overlaid on the

AICHA atlas (colored ROIs indicate homotopic regions). **B.** Proportional distribution of AICHA ROIs within WSAs across resting-state networks and subcortical regions: VIN (visual network, purple): 54.3%, SMN (somatomotor network, blue): 4.8%, DAN (dorsal attention network, green): 15.8%, SAN (salience network): 0%, LIN (limbic network, cream): 22.2%, ECN (executive control network, orange): 38.9%, DMN (default mode network, red): 10.0%, and SubCort (subcortical regions, black): 13.6%. **C** and **D.** Group-level comparisons of inter-hemispheric PSD and coherence values inside and outside WSAs for healthy controls (green) and patients with ICAS (orange). **C.** Absolute inter-hemispheric PSD differences $|\Sigma(\Delta_{LR}\ \mathrm{PSD})|$ at <0.05 Hz and ~0.1 Hz (0.08-0.1 Hz). **D.** Inter-hemispheric coherence values for homotopic and heterotopic FCs inside (left) and outside WSAs (right). **E-H.** Network-specific inter-hemispheric coherence at ~0.1 Hz (0.08-0.1 Hz) in ICAS patients: **E** and **F.** Network-wise coherence matrix (left) and corresponding circular visualizations (right) inside (**E**) and outside (**F**) WSAs. Gray color in the SAN row and column (**E**) denotes unassigned values. **G** and **H.** Group comparisons of inter-hemispheric coherence across networks inside (**G**) and outside (**H**) WSAs. Two-sample t-tests were used to assess group differences (∗: p-value<0.05, n.s.: not significant). **I** and **J.** Group comparisons of inter-hemispheric differences in quantitative MRI parameters (CBV, CBF, $CMRO_2$, and BOLD time lag) inside (**I**) and outside (**J**) WSAs. Values represent absolute sums of left–right hemisphere differences ($|\Sigma(\Delta_{LR}\ \mathrm{MRI\ Parameter})|$). Wilcoxon rank-sum tests were used to assess statistical significance (∗: p-value < 0.05, ∗∗: p-value < 0.01, and n.s.: no significance). Diamond markers and outlines indicate group means and 95% confidence intervals.

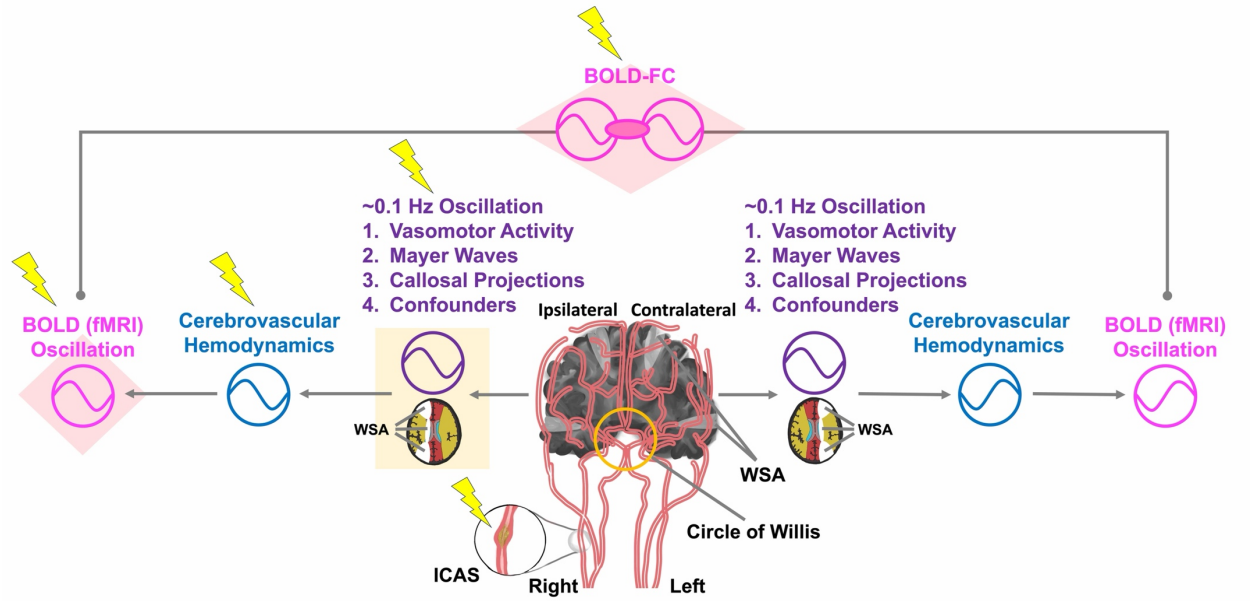

Figure 4. Interpretational cascade model of unilateral ICAS-driven cerebrovascular hemodynamics and its impact on BOLD functional connectivity (FC), inspired by the seminal work of Mateo et al. (5)**.** Unilateral internal carotid artery stenosis (ICAS, lightning symbol) may lead to impaired ~0.1 Hz oscillations transmitted through shared vascular networks, particularly via the Circle of Willis. Disrupted ~0.1 Hz oscillations, arising from vasomotor activity, Mayer waves, callosal projections, and other confounders, in the hemisphere ipsilateral to ICAS alter downstream cerebrovascular hemodynamics (e.g., cerebral blood flow, cerebral blood volume, and cerebral metabolic rate of oxygen), especially in vulnerable watershed areas (WSAs). These hemodynamic alterations result in disrupted frequency-specific BOLD oscillations and FC between two hemispheres, as measured by reduced inter-hemispheric coherence at ~0.1 Hz.